LATERAL TORSIONAL BUCKLING OF WELDED STAINLESS STEEL I-PROFILE BEAMS: EXPERIMENTAL STUDY

Maarten FORTAN[a] **and Barbara ROSSI**[a,b]

[a] Department of Civil Engineering, KU Leuven, Belgium
Jan Pieter de Nayerlaan 5, Sint-Katelijne-Waver, Belgium.
Email: maarten.fortan@kuleuven.be

[b] University of Oxford, Department of Engineering Science, UK
Emails: barbara.rossi@new.ox.ac.uk

Keywords: Stainless steel structures; Lateral torsional buckling; Digital Image Correlation; Duplex stainless steel.

Abstract. *In this paper, an experimental program is presented consisting of 13 experiments on welded stainless steel I-profile beams subjected to lateral torsional buckling, in which 11 specimens are made of the lean duplex stainless grades EN 1.4062 and EN 1.4162, while the last two specimens are made of the austenitic grade EN 1.4404. The beam heights are 160, 210 and 260 mm, and the beams have a constant flange width of 160 mm. This results in 3 different strong axis elastic section moduli, but similar weak axis bending resistances. The range of beam buckling length covers slendernesses from 0.30 to 0.76. The geometrical imperfections of the specimens were measured using digital image correlation (DIC). The web was first measured along its whole length. Then the beam was placed on its fork supports and the imperfection was then re-measured once more to check the influence of gravity and the test set-up. Traditional four-point bending tests were carried out, during which, the displacements were measured using LVDTs, inclinometers and DIC. In this paper, the measured ultimate moments, together with results of experiments collected in the literature, are compared to the design rules provided in EN 1993-1-4, for which a safe but rather conservative design is obtained, and to the recent proposal of Taras and Greiner dedicated to carbon steel beams. The latter provides better results for high slendernesses, but there is clearly room for improvement.*

1 INTRODUCTION

Over the last decade, an evolution was noticed in the methods used to predict lateral torsional buckling (LTB) failure of carbon steel I-profile beams. Some scepticism arose about the design rules in EN1993-1-1 (2005) following the works carried out by Taras and Greiner (2010) where some discrepancies were noticed when comparing the LTB curves to numerical parametric studies. These inaccuracies were particularly large for stocky sections in the high slenderness range. The authors of the study then developed a more consistent approach to predict the instability of I-profile carbon steel beams. In contrast to the approach provided EN 1993-1-1, where the well-known factor ϕ_{LT} only depends on the imperfection factor α_{LT} and lateral torsional dimensionless slenderness $\bar{\lambda}_{LT}$ combined with the plateau length $\bar{\lambda}_0$, this new approach creates individual buckling curves for each cross-section. To do so, the weak axis flexural buckling slenderness $\bar{\lambda}_z$ and the ratio of the strong-to-weak axis elastic section moduli $\frac{W_{y,el}}{W_{z,el}}$ are introduced in the calculation of ϕ_{LT} as in the following equation:

$$\phi_{LT} = 0.5\left[1 + \alpha_{LT}\left(\bar{\lambda}_z - \bar{\lambda}_0\right)\sqrt{\frac{W_{y,el}}{W_{z,el}}\frac{\bar{\lambda}_{LT}^2}{\bar{\lambda}_z^2}} + \bar{\lambda}_{LT}^2\right] \tag{1}$$

The new formulation led to pronounced improvement of the prediction of LTB failure loads of I-profile carbon steel beams, as demonstrated in (Taras, 2011) and will be introduced in the next revision of the European design rules.

The present paper tries to respond to the question if this new formulation can be used for welded stainless steel I-profile beams. To do so, the predictions of the new approach are compared to the ultimate moments obtained experimentally on 13 different stainless steel beams. New experiments had to be carried out for the reason that, until now, research on the LTB behaviour of stainless steel beams was quite scarce. Three scientific papers dealing with stainless steel can however be quoted. The first experiments were done by Van Wyk et al. (1990) on ferritic stainless steel cold-formed channel sections, spot welded back-to-back to form I-profile sections. Nevertheless, these sections are not really representative of welded I-sections manufactured from hot-rolled plates, (Fortan et al., 2016). The paper of Burgan et al. (2000) is however much more relevant to the objective of this study. In his research, 12 tests of beams (9 on austenitic beams and 3 on duplex beams) subjected to LTB were carried out. More recently, 10 tests on austenitic beams were described by Wang et al. (2014). Based on such limited information, it was, up to now, not possible to allow for another less conservative imperfection factor then the one currently proposed for all stainless steel open sections in EN 1993-1-4 (2006), which equals 0.76. Since the formulation proposed by Taras and Greiner (2010) is mainly based on the geometrical properties of the cross-sections, it should also be applicable to stainless steel which is what the present paper tries to demonstrate. Testing LTB is a tedious task which was herein achieved for two duplex stainless steel grades and one austenitic grade. To properly assess the proposed changes, various geometries were tested with different strong-to-weak axis elastic section moduli but similar weak axis bending resistances. The range of beam buckling length covered slendernesses from 0.30 to 0.76. Traditional four-point bending tests were conducted, during which digital image correlation (DIC) was used to capture the strong axis flexure and torsional displacements. Those displacements were also measured using LVDTs and inclinometers. In this paper, the measured ultimate moments, together with results of experiments collected in the literature, (Burgan et al., 2000) and (Wang et al., 2014), are compared to the design rules provided in EN 1993-1-4 and to the recent approach proposed for carbon steel beams in (Taras and Greiner, 2010).

2 EXPERIMENTAL INVESTIGATIONS

2.1 Test specimens

In total, 13 welded I-section beams made of 3 stainless steel grades were tested. Most of the specimens were made of the lean duplex grades EN 1.4062 (2202) and EN 1.4162 (2101). These grades have a relatively high strength with a nominal yield strength of 450 MPa for hot-rolled plates and an ultimate strength of 650 MPa. Moreover, both grades are classified in corrosion resistance Class 3 according to Annex A of EN 1993-1-4 (2006). This is why they are occasionally recognised as a good (economical) alternative to conventional austenitic grades in load-bearing structural elements in corrosive environments. The third grade that was tested in this study is the well-known austenitic grade EN 1.4404 (316L), which has comparable corrosion resistance but a lower nominal yield strength of 220 MPa.

An overview of the dimensions of the tested specimens is given in Table 1. Note that the notations used in Table 1 are defined in Figure 1 and Figure 4. All beams were doubly symmetric welded I-profiles. They were all tested in a four-point bending test configuration and were simply supported. Stiffeners of 10 mm thick were located above the supports and at the loading points. The widths b_f of all beams were kept constant, but their height-to-width ratio was varied between 1.0, 1.3 and 1.6. Several buckling lengths per studied cross-section were tested to cover a slenderness range from 0.30 to 0.76. The beams made of the stainless steel grades EN 1.4162 and EN 1.4404 were welded by Stalatube Oy, in Finland, while the beams made of the grade EN 1.4062 were welded in the Welding Centre of Campus De Nayer, KU Leuven. For all beams, gas metal arc welding (GMAW) was used with the following consumables: EN ISO 14343: 19 12 3 L Si for EN 1.4404, EN ISO 14343: 22 9 3 N L for EN 1.4162 and EN ISO 14343: 23 7 N L for EN 1.4062. In the Welding Centre of Campus De Nayer, KU Leuven, a complete new set-up, visible in Figure 2, was designed and built to semi-automatically weld both sides of the profile web to its flange at the same time, minimising cross-section distortion while increasing the welding time efficiency.

2.2 Test set-up

The test set-up for one typical beam is shown in Figure 3, with indication of the locations of the used measurement devices in Figure 4. During the tests, two Enerpac RC7513 hydraulic jacks, with a maximum load of 750 kN and a stroke of 333 mm, were controlled by one hydraulic pump to generate two equal point loads, which are measured separately by one load cell per jack. A distribution beam was used to avoid lateral loads on the jacks and load cells, when large deformations occur in the tested beam. The load was applied with an approximate speed of 2 kN/s with pauses every 20 kN to ensure a static behaviour. The fork-end supports were specifically designed for these tests to ensure the lateral stability of the beam, while still being flexible in height and position to accommodate different cross-section geometries, as shown in Figure 5. In addition, to guarantee the stability of the jacks during the test, lateral sliding supports were used at the level of the loading points, visible in Figure 6. The first part was a truss-system connected to both the floor and the loading frame, which ensured a stiff basis to slide on. The second part established the connection between the tested beam and the column using a high-modulus polyethylene plate to minimize friction.

LVDTs were placed at the loading points – LVDT 1 and 2 in Figure 4 – to measure the vertical displacement of the beam at the loading points. The displacements of each support were also controlled using LVDT 3 to 8, see Figure 4. Divided over the buckling length L_b in between the lateral supports, 9 x 3 inclinometers were fixed onto the web and flanges to follow the inclination along the tested beam. The inclinometers, which are based on accelerometers and described in detail in (Lauwens et al., 2019), are only used during the pauses to avoid a dynamic effect on their measurements. The displacement of the web in between the two lateral supports was followed using stereo vision digital image correlation (DIC). This optical measurement technique uses two cameras to triangulate each subset of a speckle pattern usually painted onto the measured surface and to generate a full 3D point cloud of the pattern. The comparison of subsequent patterns during the test allows to compute a deformed surface. To optimize the contrast of the pattern, a white primer was painted on the web. Afterwards, an optimized black pattern was applied by transferring it from a laser printed paper on the web using acetone. Pictures were taken with two AVT cameras with 12 mm lenses before every test to determine the imperfection shape and amplitude of each specimen as will be described in Section 3.2. During the test, synchronized pictures were taken at 0.1 Hz to follow the in- and out-of-plane deformations in the mid-span region of the beam.

3 TEST RESULTS

3.1 Material behaviour

The material behaviour of the three studied stainless steel grades was determined via uniaxial tensile tests according to EN ISO 6892 (2009). The tensile tests were carried out on an Instron HDX 1500 kN machine with a constant strain rate of 0.00025 s^{-1}. For both duplex stainless steel grades, EN 1.4062 and EN 1.4162, three coupons were extracted from the hot-rolled plate in the rolling direction and three coupons in the transverse direction. An exception was made for the 10 mm plate of EN 1.4162, where only coupons in the rolling direction were available. For the austenitic grade, EN 1.4404, no extra material for coupons remained. Therefore, one coupon was manufactured from the web of one beam (I256x160Lb1300_EN1.4404) in the unloaded part, outside of the supports, in the transverse direction of the plate.

Both the engineering strain and the true strain were measured using DIC. The engineering stress-strain curves, presented in Figure 7, were used to determine the main material characteristics and Ramberg-Osgood's parameters, provided in Table 2. The measured Young's modulus is, on average, 2 % higher than the nominal value of 200 GPa provided in EN1993-1-4. Whereas for the yield and ultimate strengths, the overstrength was significantly higher with, on average, respectively 18 % and 12% for the duplex grade and 31% and 22% for the austenitic grade. The Ramberg-Osgood parameter n, describing the roundness of the curve below the yield stress, is similar to the recommended value of 8 presented in (Arrayago et al., 2015) for duplex stainless steel, but for austenitic, the recommended value of 7 is slightly higher than the one found in the experiment. The true strain measurements, presented in Figure 8 and Figure 9, are in good agreement with the calculated ones based on the engineering strain in the initial stage up to 10%.

3.2 Imperfections

LTB is a global instability phenomenon and is therefore influenced by the initial imperfections of the beam. Two important imperfections are presently discussed, specifically the residual stresses and the geometrical imperfections. Firstly, the residual stresses are induced during welding due to uneven cooling of the weld and its surrounding zones. Although no residual stress measurements were performed in this study, it is worth pointing Yuan et al.'s residual stress model for ferritic, austenitic and duplex stainless steel based on extensive measurements of welded I-sections as well as closed box sections, presented in (Yuan et al., 2014). Secondly, the geometrical imperfections or initial shapes of the tested specimens, were presently measured before each experiment. The main imperfection influencing the global stability is the straightness (bow imperfection) of the beam. This imperfection was measured using DIC over the full surface of the web of the beam, which resulted in a 3D point cloud of the web, visible as *imperfection 1* in Figure 10 and Figure 11 for two typical beams. To minimize the influence of noise on the correlation in the pictures, 100 static pictures were taken for each beam. For each pixel, the median grey value of 50 pictures was used, resulting in two pictures with reduced noise. They were used for the correlation of the point cloud in the software MatchID and led to the graphic representation of the web shape along each beam. An overview of all the measured shapes can be seen in Figure 12. The shapes for all specimens were quite similar to the bow imperfection described in EN 1090 (2009). The imperfection amplitudes for each beam are provided in Table 3, presented as the sweep at the top ($\Delta_{1,top}$) and bottom of the web ($\Delta_{1,bot}$) along the length of the beam and the average imperfection in between the lateral supports ($\delta_{1,avg}$).

A second imperfection measurement, *imperfection 2,* was then carried out at the start of each LTB experiment. The same procedure as for *imperfection 1* was followed but based on pictures taken of the specimen already in place on the testing set-up, which is why only part of the web is visible due to the position of the lateral supports, and therefore subjected to its own weight. When compared to *imperfection 1*, minor differences could be noticed for most specimens. Figure 11 shows the obtained difference for I260x160Lb2200_EN1.4162. This difference is most likely caused by the use of different boundary conditions in the two measurements. In the first measurement, the beams are supported over the length of the beam with no lateral restraints, while in the second measurement, the beam is supported at the fork supports and laterally restraint at the fork supports and lateral supports.

3.3 Lateral torsional buckling

A global LTB failure mode involving minor axis bending and torsion was observed for all specimens, visualized in Figure 13. In Table 4, the ultimate load P_{ul} and ultimate moment M_{ul}, the maximum vertical displacement at the loading points $U_{y,ul,LP}$, the maximum rotation at the mid-span $\theta_{x,ul,Mid}$ and the maximum translation at the mid-span $U_{z,ul,Mid}$ are provided. To evaluate the dimensionless slenderness $\bar{\lambda}_{LT}$, the elastic critical moment M_{cr} was obtained numerically through a linear buckling analysis. Together with the elastic material properties and the geometry of the section, the boundary conditions have a major influence on the critical moment. However, lateral movements and rotations also occurred close to the lateral supports during the experiments, causing a higher actual slenderness for the beams. An overview of the translations and rotations measured close to the supports at ultimate load is given in Table 5. To approximate the critical moment, the somewhat imperfect behaviour of the lateral supports was introduced in the FE model using constraint equations at the nodes close to the lateral supports where these movements and rotations were measured. These definite relations ensure that these nodes behave as during the experiment. Since these displacements and rotations were precisely measured, they can be related to the same degrees of freedom located at mid-span, the constraint was therefore such that those are in the same proportion in the FEM (i.e. as those in the middle of the beam measured at ultimate load). This approach ensures that the more flexible behaviour of the lateral supports is accounted for in the FEM and that comparable buckling modes are obtained. Furthermore, the elastic critical moment and the corresponding dimensionless slenderness $\bar{\lambda}_{LT}$ are calculated using the measured Young's modulus as well as yield strength.

Figure 14 presents the evolution of the average vertical displacement at the loading points and the maximum lateral translation in the middle compared to the imposed moment for all specimens. Furthermore, the full out-of-plane displacement field of the web measured with DIC is shown in Figure 15 for beam I214x162Lb1600_EN1.4062. The corresponding moment-vertical displacement curve for the same beam is shown in Figure 16. At point A, the beam is deforming elastically, no instability occurred yet and therefore the out-of-plane (z-)displacements are negligible. Through points B and C and then, for the ultimate moment at point D, the out-of-plane torsional deformations increase, and the LTB failure mode becomes visible with out-of-plane (z-)translations and (x-)rotations happening in the middle part of the beam.

The out-of-plane displacements at the ultimate load are shown in Figure 17 for all beams. Lateral torsional buckling failure in between the two lateral supports is clearly visible for all the tested specimens.

4 COMPARISON AGAINTS CURRENT DESIGN PREDICTIONS

The design rules for LTB of stainless steel beams in EN 1993-1-4 (2006) (summarized by equations 3 to 6) differ from those in EN 1993-1-1 (2005) in the used imperfection factor α_{LT} and plateau length $\bar{\lambda}_0$. For stainless steel, a plateau length of 0.4 is prescribed, compared to 0.2 for carbon steel. For the imperfection factor, the most conservative value of 0.76 is currently recommended for all open sections made of stainless steel. The carbon steel design rules however propose both 0.49 and 0.76 depending on the height-to-width ratio of the cross-section. One last difference to point is the safety factor γ_{M1}, which is 1.10 for stainless steel and 1.0 for carbon steel.

$$\bar{\lambda}_{LT} = \sqrt{\frac{W_y f_y}{M_{cr}}} \tag{3}$$

$$\phi_{LT} = 0.5\left[1 + \alpha_{LT}\left(\bar{\lambda}_{LT} - \bar{\lambda}_0\right) + \bar{\lambda}_{LT}^2\right] \tag{4}$$

$$\chi_{LT} = \frac{1}{\phi_{LT} + \sqrt{\phi_{LT}^2 - \bar{\lambda}_{LT}^2}} \leq 1.0 \tag{5}$$

$$M_{b,Rd} = \chi_{LT} \frac{W_y f_y}{\gamma_{M1}} \qquad (6)$$

The recent proposal of Taras and Greiner (2010) is mainly ruled by the calculation of ϕ_{LT}, as already indicated in the first equation of this paper, where the normalized slenderness for weak axis flexural buckling for the unbraced length of the compression flange $\bar{\lambda}_z$ and the ratio of the strong-to-weak axis elastic section moduli $W_{y,el}/W_{z,el}$ are included. The proposal uses a plateau length of 0.2 for carbon steel beams and an imperfection factor α_{LT} equal to 0.21 for welded cross-sections. In the proposal, the factor $\alpha_{LT}\sqrt{W_{y,el}/W_{z,el}}$ is also limited to 0.64.

In Figure 18, the normalised ultimate resistances of the tested beams are compared to the predictions of EN 1993-1-4 and Taras and Greiner (2010), where the ultimate bending moment obtained experimentally is compared to the predicted one. It is clear that the predictions are on the safe side and that there is plenty of room for improvements of the design rules for stainless steel beams suffering LTB. Beams with a slenderness lower than 0.6, show slightly improved predictions of their resistances when calculated using the current European design rules. The main cause is the plateau length $\bar{\lambda}_0$ which is set to 0.2 in the proposal of Taras and Greiner compared to 0.4 in EN 1993-1-4. However, for a higher slenderness, the equation of Taras and Greiner gives slightly better predictions. When comparing the predictions with the experimental strengths, the design rules of EN 1993-1-4 have a rising conservatism with an increasing slenderness, while the conservatism of the predictions by Taras and Greiner remains approximately constant.

5 CONCLUSION

In this paper, an experimental program consisting of 13 beams suffering lateral torsional buckling (LTB) is presented. Our intention was to widen the experimental basis necessary to assess the accuracy of the current design rules available in EN 1993-1-4 (2006) for stainless steel beams suffering LTB. In the present study, 11 experiments were done on lean duplex stainless steel (EN 1.4062 and EN 1.4162) welded beams and on 2 austenitic (EN1.4404) welded beams. The widths of all the beams were kept constant, but the height-to-width ratio was varied between 1.0, 1.3 and 1.6. Several buckling lengths per studied cross-section were tested to cover a slenderness range from 0.30 to 0.76.

The specimens were manufactured in two groups. The first group of beams, which contains the grades EN 1.4162 and EN 1.4404, was welded by an industrial company named Stalatube Oy, while the second group was welded on-site in the Welding Centre of Campus De Nayer, KU Leuven. The initial imperfection shape of each beam was measured using DIC, leading to a representation of the shape and amplitude of the imperfection along the beam for all specimens. It is worth noting that, although the measured initial geometric imperfection amplitudes were rather big, no significant differences were noticed between the two groups.

All specimens had an LTB failure mode which could be captured using LVDTs at various points along the beam, inclinometers all along the beam's buckling length as well as DIC. When compared to predictions made according to EN 1993-1-4, and Taras and Greiner (2010), strong conservativeness was noticed with an average experimental-to-predicted strength ratio of 1.22 for EN 1993-1-4 and 1.26 for Taras and Greiner. For the beam with the highest slenderness, the recent proposal showed better predictions which is comparable to what was found for carbon steel beams in the higher slenderness domain.

The present experimental campaign is used in a companion paper (Fortan and Rossi, 2020) to validate a finite element model followed by a parametric study of stainless steel beams suffering LTB. Based on the parametric study, new recommendations are proposed and a complete reliability assessment according to Annex D of EN 1990 is carried out to demonstrate that the safety factors are in agreement with the codified value of 1.10 for stainless steel.

DATA AVAILABILITY STATEMENT

Some or all data, models, or code that support the findings of this study are available from the corresponding author upon reasonable request.

ACKNOWLEDGEMENT

The first author is funded by a PhD fellowship from the Research Foundation Flanders. Outokumpu, Stalatube Oy and Industeel are gratefully acknowledged for their help during this study.

REFERENCES

Arrayago, I., Real, E. and Gardner, L. 2015. Description of stress-strain curves for stainless steel alloys. Materials and Design, Volume 87, Pages 540-552.

Burgan, B.A., Baddoo, N.R. and Gilsenan, K.A. 2000. Structural design of stainless steel members comparison between Eurocode 3, Part 1.4 and test results. Journal of Constructional Steel Research, 54, 51-73.

European Committee for Standardization (CEN). 2005. Eurocode 3: design of steel structures - part 1-1: General rules and rules for buildings. Brussel, 2005(+AC:2009)/A1:2014.

European Committee for Standardization (CEN). 2006. Eurocode 3: design of steel structures - part 1-4: General rules - Supplementary rules for stainless steels. Brussel, 2006/A1:2015.

European Committee for Standardization (CEN). 2009. EN ISO 6892 Metallic materials – Tensile testing – Part 1: Method of test at room temperature. Brussel, 2009.

European Committee for Standardization (CEN).2018. EN 1090-2 Execution of steel structures and aluminium structures – Part 2: Technical requirements for steel structures. Brussel, 2018.

Fortan, M., Zhao, O. and Rossi, B. 2016. Lateral torsional buckling of welded duplex stainless steel I section beams. Proceedings of the Sixth International Conference on Structural Engineering, Mechanics and Computation 2016. Cape Town, South Africa.

Fortan, M. and Rossi, B. 2020. Lateral torsional buckling of welded stainless steel I-profile beams: design and reliability. Journal of Structural Engineering

Lauwens, K., Fortan, M., De Weerdt, J., Pelgrims, P. and Rossi, B. 2019. The use of inclinometers and DIC to measure the rotation in full-scale tests on construction elements. Proceedings of the international colloquium on stability and ductility of steel structures 2019. Prague, Czech Republic.

Taras, A. and Greiner, R. 2010. New design curves for lateral-torsional buckling - Proposal based on a consistent derivation. Journal of Constructional Steel Research, Volume 66, pages 648-663.

Taras, A. 2011. Contribution to the development of consistent stability design rules for steel members. Graz University of Technology. PhD thesis.

Van Wyk, M.L., Van den Berg, G.J. and Van der Merwe, P. 1990. Lateral torsional buckling strength of doubly symmetric stain-less steel beams. International Specialty Conference on Cold-Formed Steel Structures, 493-504.

Wang, Y.Q., Yang, L., Gao, B., Shi, Y.J. and Yuan, H.X. 2014. Experimental Study of Lateral-torsional Buckling Behavior of Stainless Steel Welded I- section Beams. International Journal of Steel Structures, 14, 411-420.

Yuan, H.X., Wang, Y.Q., Shi, Y.J. and Gardner, L. 2014. Residual stress distributions in welded stainless steel sections. Thin-Walled Structures, Volume 79, Pages 38-51.

Tables:

Table 1: Dimensions of the tested beams

Table 2: Tensile test results

Table 3: Measured imperfection amplitudes, where Δ is the imperfection over the whole length of the beam and δ represents the imperfection between the lateral supports.

Table 4: Overview of the test results

Table 5: Lateral movement and rotation measured close to the lateral supports at ultimate load.

Table 1: Dimensions of the tested beams

Name	Material	h_w mm	b_f mm	t_w mm	t_f mm	L_{tot} mm	L_{net} mm	L_b mm
I159x160Lb1000_EN1.4162	EN 1.4162	139	160	10.0	8.0	2200	2000	1000
I160x160Lb1500_EN1.4162	EN 1.4162	140	160	10.0	8.0	2700	2500	1500
I160x160Lb1800_EN1.4162	EN 1.4162	140	160	10.0	8.0	3000	2800	1800
I259x160Lb1100_EN1.4162	EN 1.4162	239	160	10.0	8.0	2500	2280	1100
I260x160Lb2200_EN1.4162	EN 1.4162	240	160	10.0	8.0	3400	3200	2200
I260x160Lb2800_EN1.4162	EN 1.4162	240	160	10.0	8.0	4000	3800	2800
I212x161Lb1250_EN1.4062	EN 1.4062	192	161	10.2	8.3	2450	2280	1250
I214x162Lb1600_EN1.4062	EN 1.4062	194	162	10.2	8.3	2800	2580	1600
I212x160Lb2000_EN1.4062	EN 1.4062	192	160	10.2	8.3	3200	2980	2000
I260x161Lb1100_EN1.4062	EN 1.4062	240	161	10.2	8.3	2500	2280	1100
I263x161Lb2000_EN1.4062	EN 1.4062	243	161	10.2	8.3	3200	3010	2000
I256x160Lb1300_EN1.4404	EN 1.4404	240	160	8.2	8.2	2500	2320	1300
I253x160Lb2200_EN1.4404	EN 1.4404	237	160	8.2	8.2	3400	3210	2200

Table 2: Tensile test results

Material	Thickness mm	Direction	E_0 MPa	$\sigma_{0.2}$ MPa	$\sigma_{1.0}$ MPa	σ_u MPa	ε_u	n	m	$n'_{0.2,1.0}$
EN 1.4062	8	Rolling	205969	515	575	726	0.248	8.5	3.5	3.3
EN 1.4062	8	Transverse	222101	560	617	754	0.204	10	3.4	2.6
EN 1.4062	10	Rolling	200426	505	561	715	0.265	8.0	3.5	2.6
EN 1.4062	10	Transverse	217112	532	584	730	0.225	8.5	3.1	2.4
EN 1.4162	8	Rolling	192527	518	566	714	0.248	8.5	3.0	3.5
EN 1.4162	8	Transverse	210765	575	610	734	0.208	10.5	2.7	2.1
EN 1.4162	10	Rolling	192952	525	579	728	0.239	8	3.1	2.5
EN 1.4404	8	Transverse	193323	288	331	633	0.428	5.5	2.2	1.9

Table 3: Measured imperfection amplitudes, where Δ is the imperfection over the whole length of the beam and δ represents the imperfection between the lateral supports.

Name	$\Delta_{1,top}$ mm	$\Delta_{1,bot}$ mm	$\delta_{1,avg}$ mm	$\delta_{2,avg}$ mm
I159x160Lb1000_EN1.4162	2.1	2.1	0.5	0.8
I160x160Lb1500_EN1.4162	2.4	2.7	0.8	1.3
I160x160Lb1800_EN1.4162	5.0	4.9	1.8	2.0
I259x160Lb1100_EN1.4162	2.3	2.3	0.4	1.5
I260x160Lb2200_EN1.4162	6.7	7.3	3.4	1.2
I260x160Lb2800_EN1.4162	/	/	/	13.0
I212x161Lb1250_EN1.4062	5.1	5	1.2	1.2
I214x162Lb1600_EN1.4062	5.5	5.2	2.4	6.4
I212x160Lb2000_EN1.4062	8.4	8.7	3.8	2.2
I260x161Lb1100_EN1.4062	4.3	4.6	0.8	2.4
I263x161Lb2000_EN1.4062	6.6	7.4	2.2	2.2
I256x160Lb1300_EN1.4404	4.0	4.0	1.0	3.6
I253x160Lb2200_EN1.4404	7.0	6.4	3.2	1.0

Table 4: Overview of the test results

Name	M_{cr} kNm	$\bar{\lambda}_{LT}$ -	P_{ul} kN	M_{ul} kNm	$U_{y,ul,LP}$ mm	$\theta_{x,ul,Mid}$ °	$U_{z,ul,Mid}$ mm
I159x160Lb1000_EN1.4162	1427	0.30	650	163	60.8	6.0	19.0
I160x160Lb1500_EN1.4162	642	0.45	588	147	59.5	4.9	21.5
I160x160Lb1800_EN1.4162	691	0.43	557	139	63.4	10.5	40.7
I259x160Lb1100_EN1.4162	2225	0.33	1012	299	52.1	2.4	13.1
I260x160Lb2200_EN1.4162	868	0.52	986	246	33.3	7.2	31.5
I260x160Lb2800_EN1.4162	415	0.76	797	199	26.0	9.1	38.6
I212x161Lb1250_EN1.4062	1035	0.42	903	232	33.6	3.0	15.7
I214x162Lb1600_EN1.4062	896	0.45	909	223	40.1	6.4	28.5
I212x160Lb2000_EN1.4062	680	0.52	754	185	32.7	9.0	33.7
I260x161Lb1100_EN1.4062	2131	0.33	1026	303	37.1	4.2	20.5
I263x161Lb2000_EN1.4062	848	0.53	968	244	22.1	6.4	30.3
I256x160Lb1300_EN1.4404	1340	0.29	575	147	31.6	5.1	22.9
I253x160Lb2200_EN1.4404	588	0.43	479	121	34.4	7.7	40.1

Table 5: Lateral movement and rotation measured close to the lateral supports at ultimate load.

Name	Lateral movement			Rotation		
	distance from lateral support	$U_{z,left}$	$U_{z,right}$	distance from lateral support	$\theta_{x,left}$	$\theta_{x,right}$
	mm	mm	mm	mm	°	°
I159x160Lb1000_EN1.4162	75	7.0	6.6	100	1.4	1.3
I160x160Lb1500_EN1.4162	60	3.4	11.5	50	1.2	3.9
I160x160Lb1800_EN1.4162	150	12.8	10.3	100	1.2	2.3
I259x160Lb1100_EN1.4162	100	7.1	2.6	50	0.4	0.7
I260x160Lb2200_EN1.4162	125	4.9	3.6	100	1.0	1.7
I260x160Lb2800_EN1.4162	145	10.9	5.3	25	2.4	1.1*
I212x161Lb1250_EN1.4062	60	6.9	6.0	25	0.9	0.5
I214x162Lb1600_EN1.4062	75	9.7	10.4	100	1.5	0.7
I212x160Lb2000_EN1.4062	70	5.8	9.3	200	1.7	2.0
I260x161Lb1100_EN1.4062	90	8.9	7.1	50	1.1	0.9
I263x161Lb2000_EN1.4062	75	7.1	8.9	200	2.2	2.4
I256x160Lb1300_EN1.4404	75	4.1	6.9	50	1.3	0.7
I253x160Lb2200_EN1.4404	65	9.5	6.5	100	0.2	1.0

*measured at 145 mm from lateral support

Figures:

Figure 1: Overview of tested sections.

Figure 2: Welding set-up used at campus De Nayer, KU Leuven.

Figure 3: Test set-up for LTB.

Figure 4: Measurement set-up for LTB.

Figure 5: Adaptable fork support.

Figure 6: Lateral support with truss system, steel connection piece and HMPE sliding plate.

Figure 7: Engineering stress - engineering strain curves.

Figure 8: Calculated true stress - measured true strain curves

Figure 9: Comparison between the different strain measurements for two typical austenitic (EN 1.4404) and duplex specimens (EN 1.4062)

Figure 10: Measured imperfection of I212x161Lb1250_EN1.4062: a) contours of the initial shape in DIC, and b) graph of the out-of-plane imperfection along the length of the beam.

Figure 11: Measured imperfection of I260x160Lb2200_EN1.4162: a) contours of the initial shape in DIC, and b) graph of the out-of-plane imperfection along the length of the beam.

Figure 12: Measured imperfection shapes.

Figure 13: Overview of failed specimens.

Figure 14: Overview of the displacement of the loading points compared to the applied moment for all tests.

Figure 15: Out-of-plane displacement during test I214x162Lb1600_EN1.4062

Figure 16: Vertical displacement of the loading points compared to the applied moment for I214x162Lb1600_EN1.4062

Figure 17: Out-of-plane displacement measured with DIC for all beams at ultimate load.

Figure 18: Comparison of the ultimate moment to the predicted moment according to EN 1993-1-4 and Taras and Greiner.

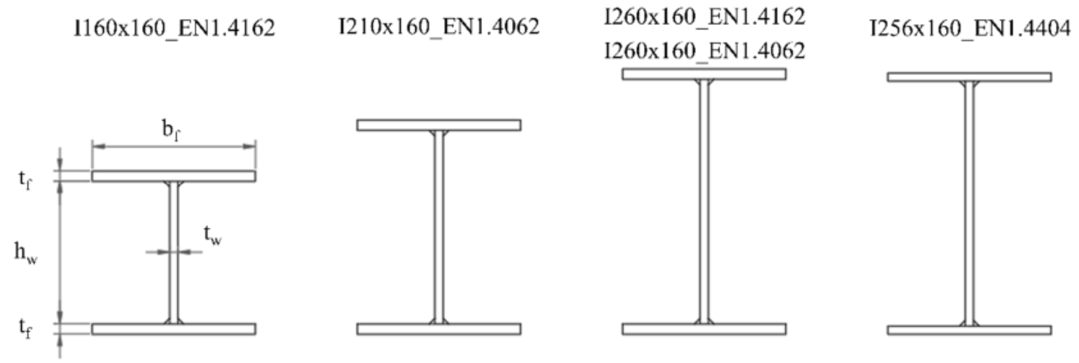

Figure 1: Overview of tested sections.

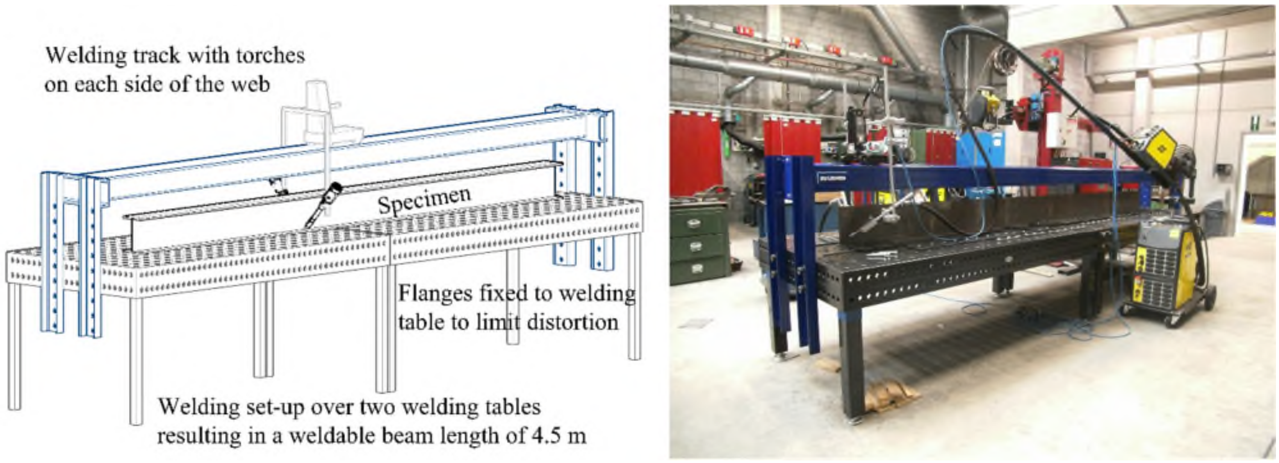

Figure 2: Welding set-up used at campus De Nayer, KU Leuven.

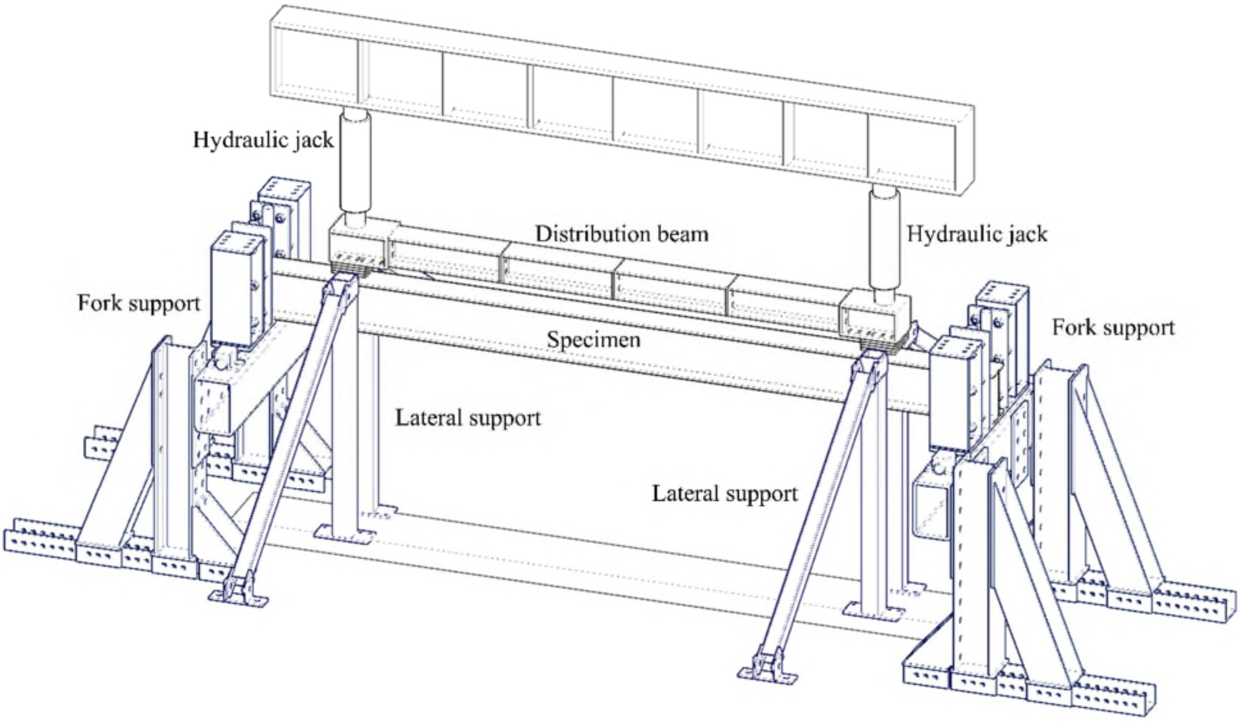

Figure 3: Test set-up for LTB.

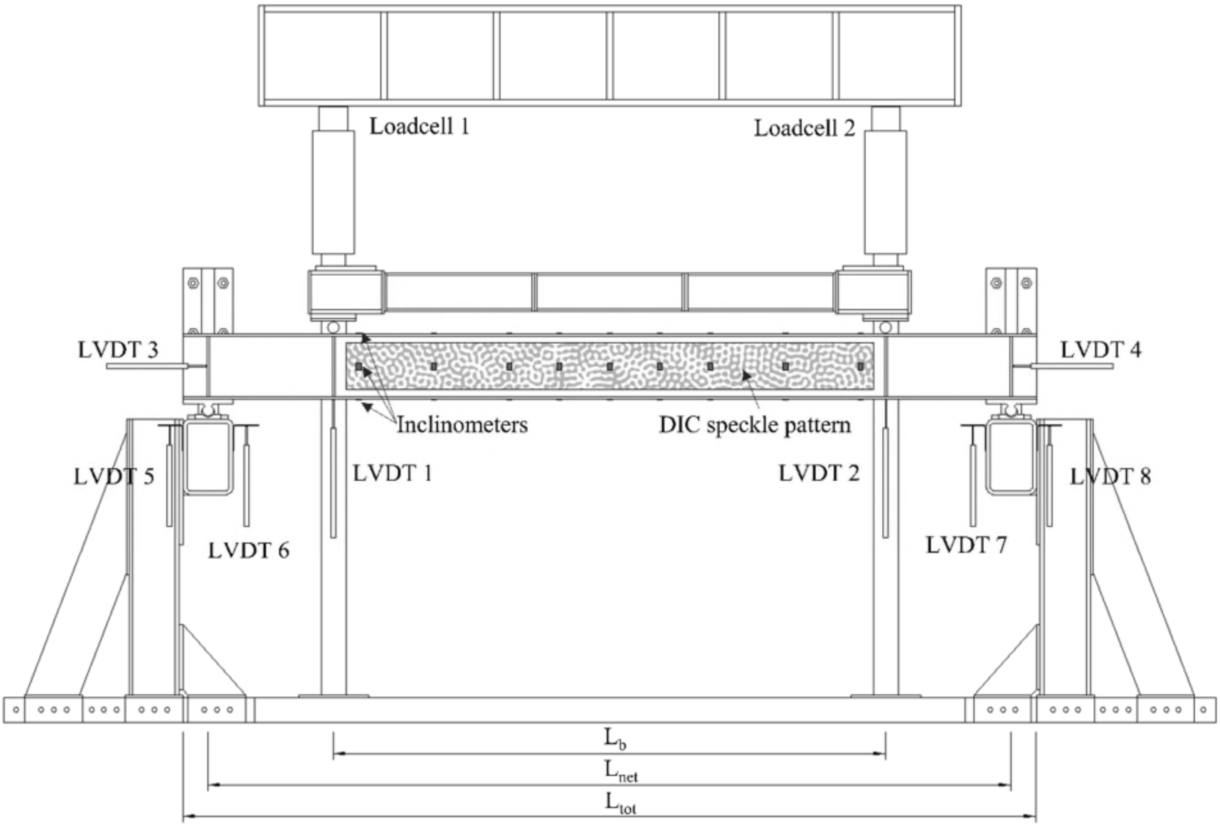

Figure 4: Measurement set-up for LTB.

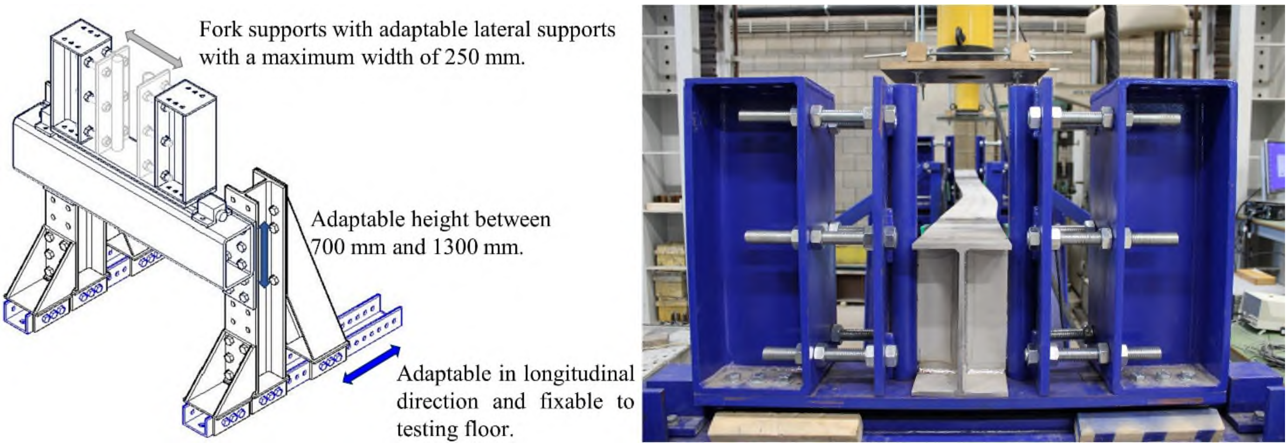

Figure 5: Adaptable fork support.

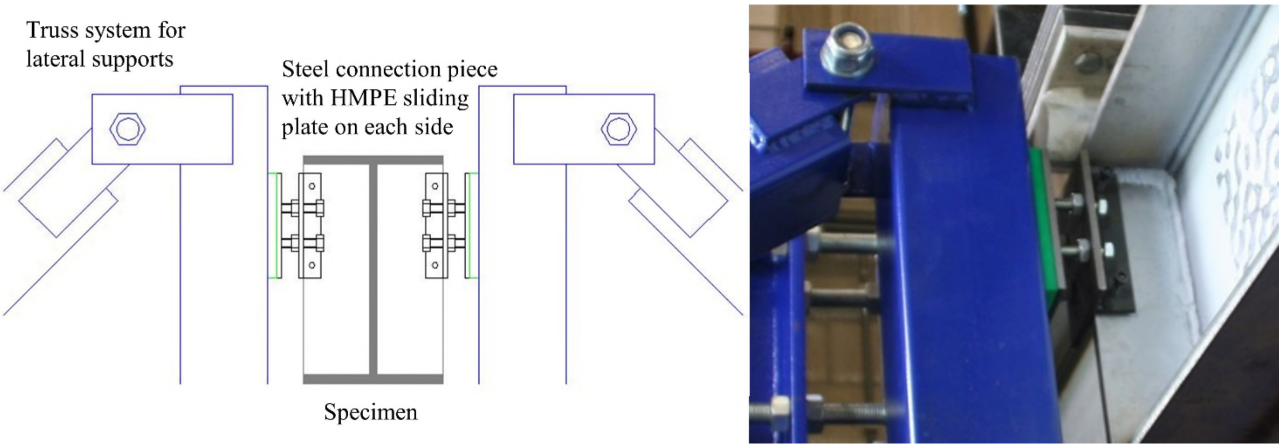

Figure 6: Lateral support with truss system, steel connection piece and HMPE sliding plate.

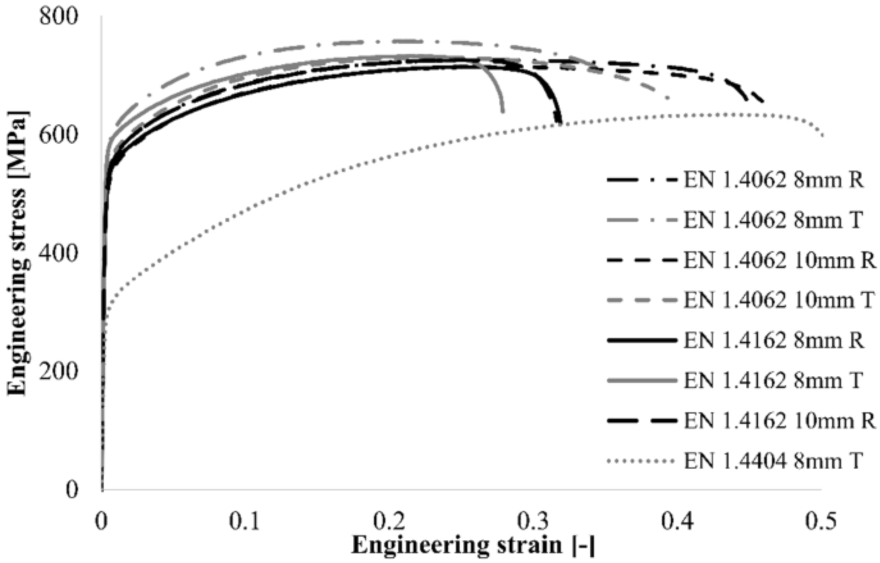

Figure 7: Engineering stress - engineering strain curves.

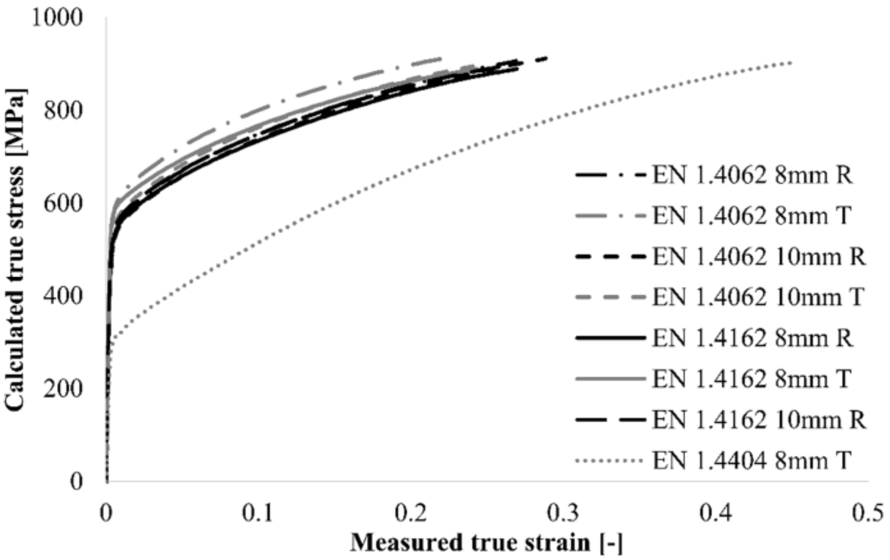

Figure 8: Calculated true stress - measured true strain curves

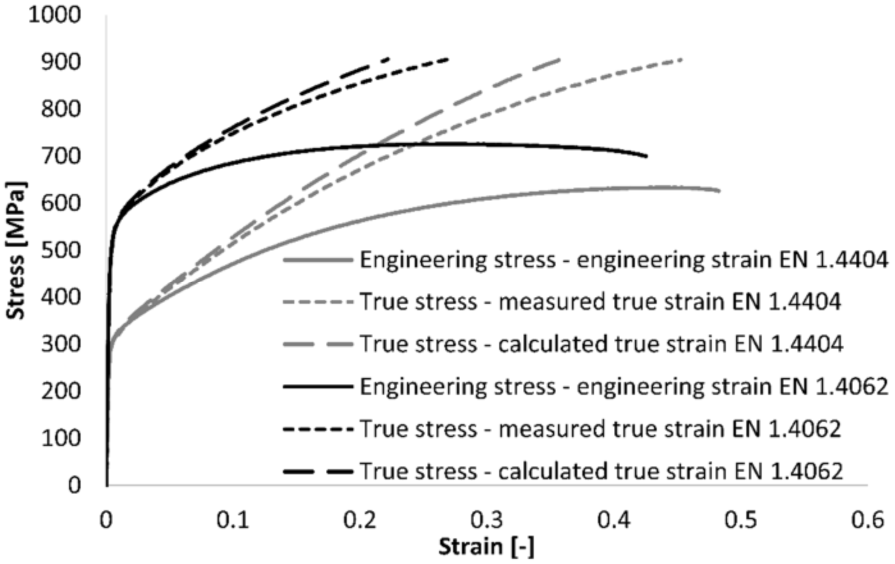

Figure 9: Comparison between the different strain measurements for two typical austenitic (EN 1.4404) and duplex specimens (EN 1.4062)

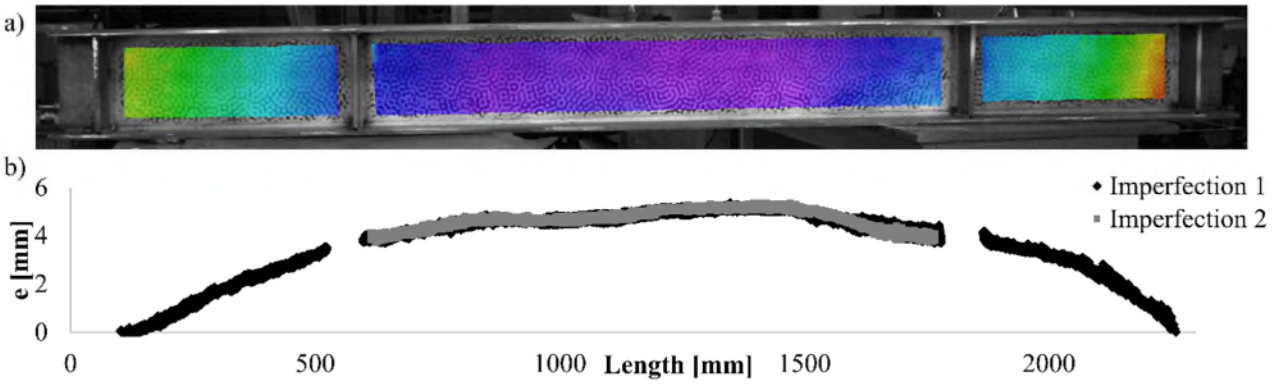

Figure 10: Measured imperfection of I212x161Lb1250_EN1.4062: a) contours of the initial shape in DIC, and b) graph of the out-of-plane imperfection along the length of the beam.

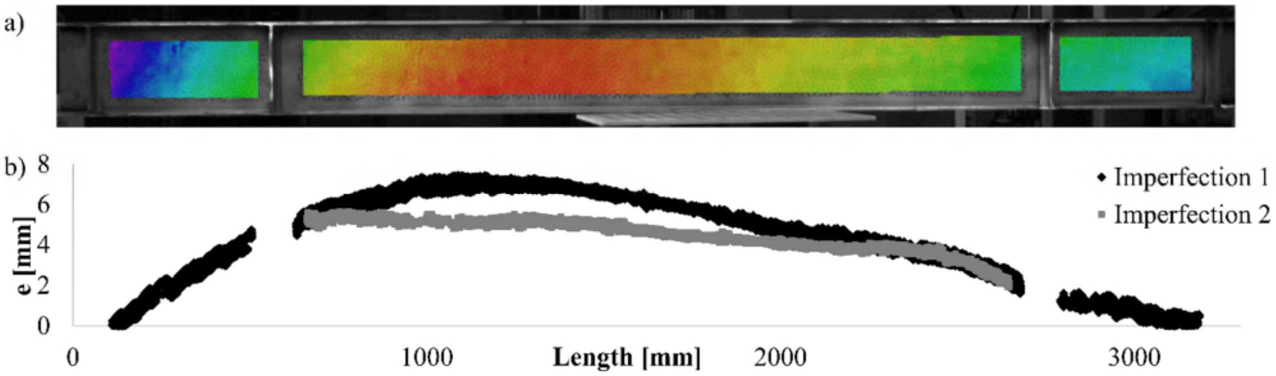

Figure 11: Measured imperfection of I260x160Lb2200_EN1.4162: a) contours of the initial shape in DIC, and b) graph of the out-of-plane imperfection along the length of the beam.

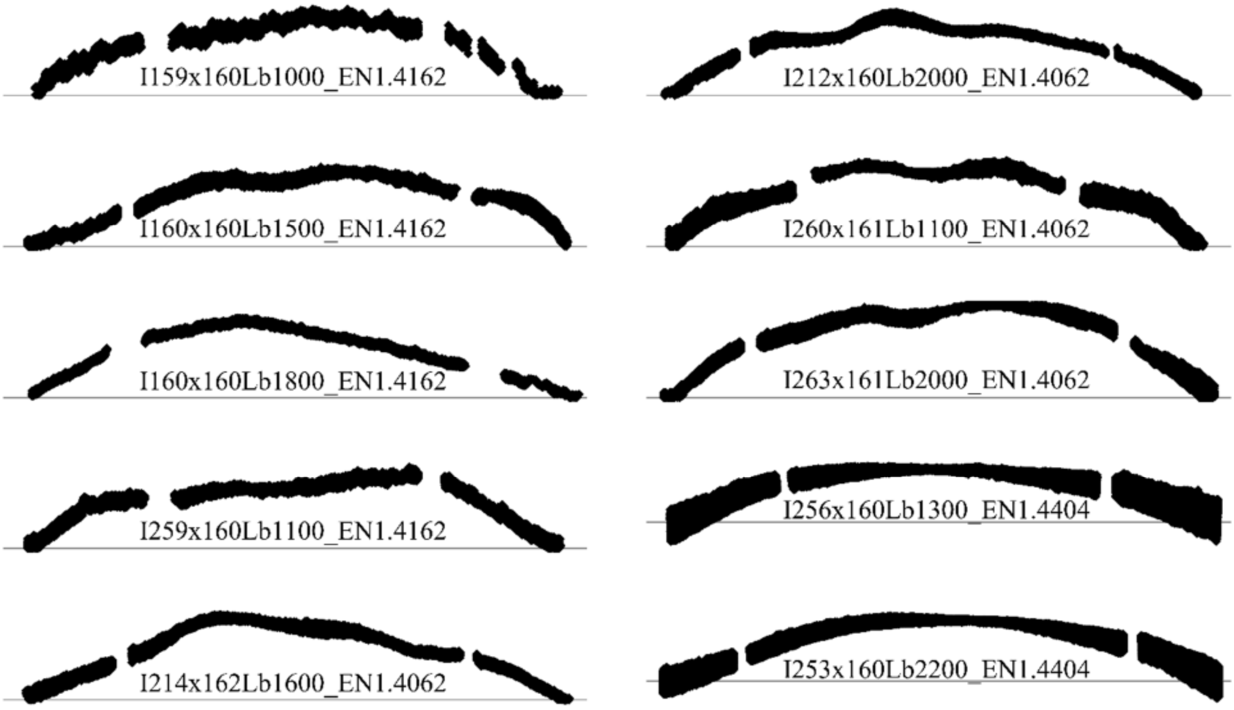

Figure 12: Measured imperfection shapes.

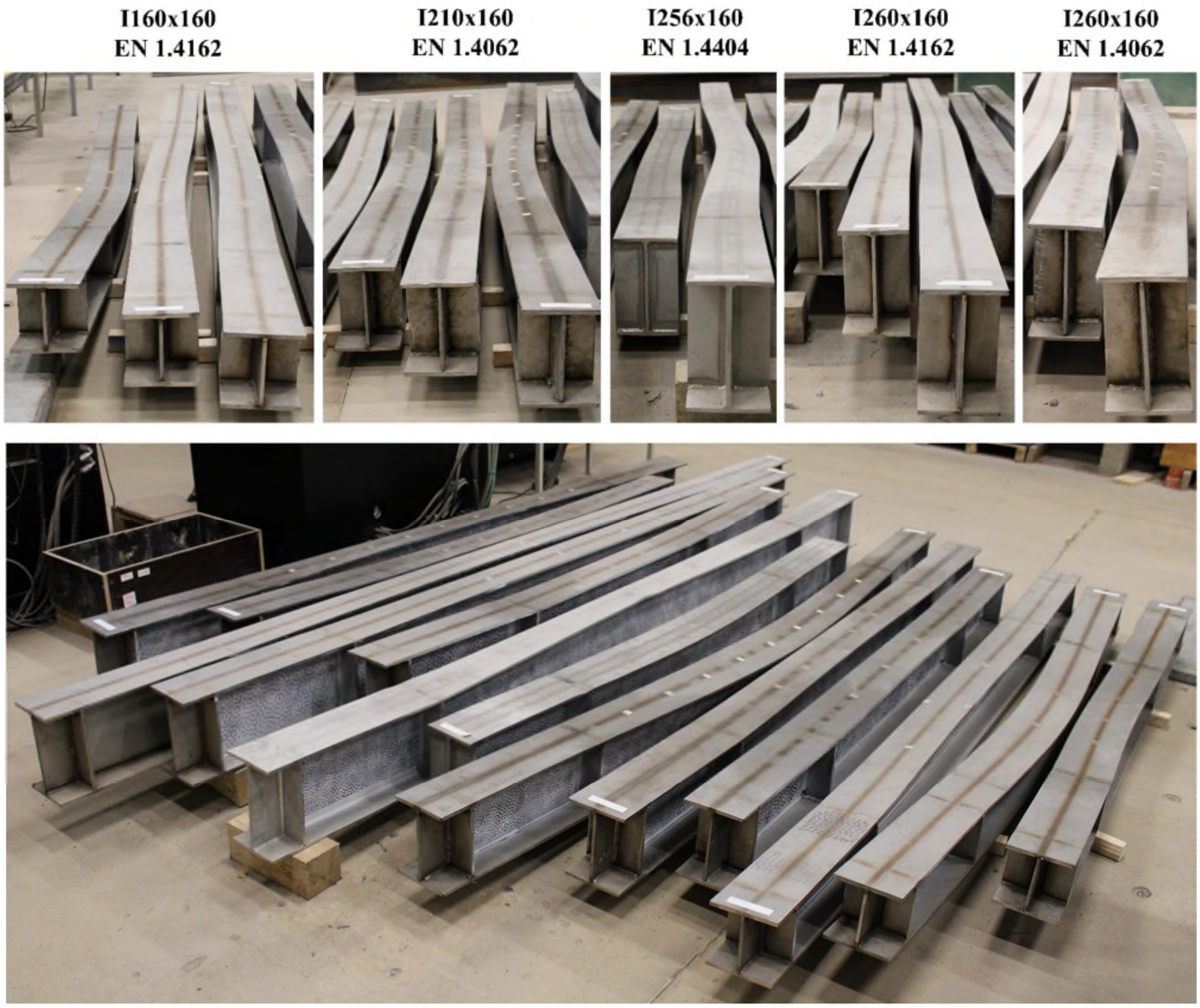

Figure 13: Overview of failed specimens.

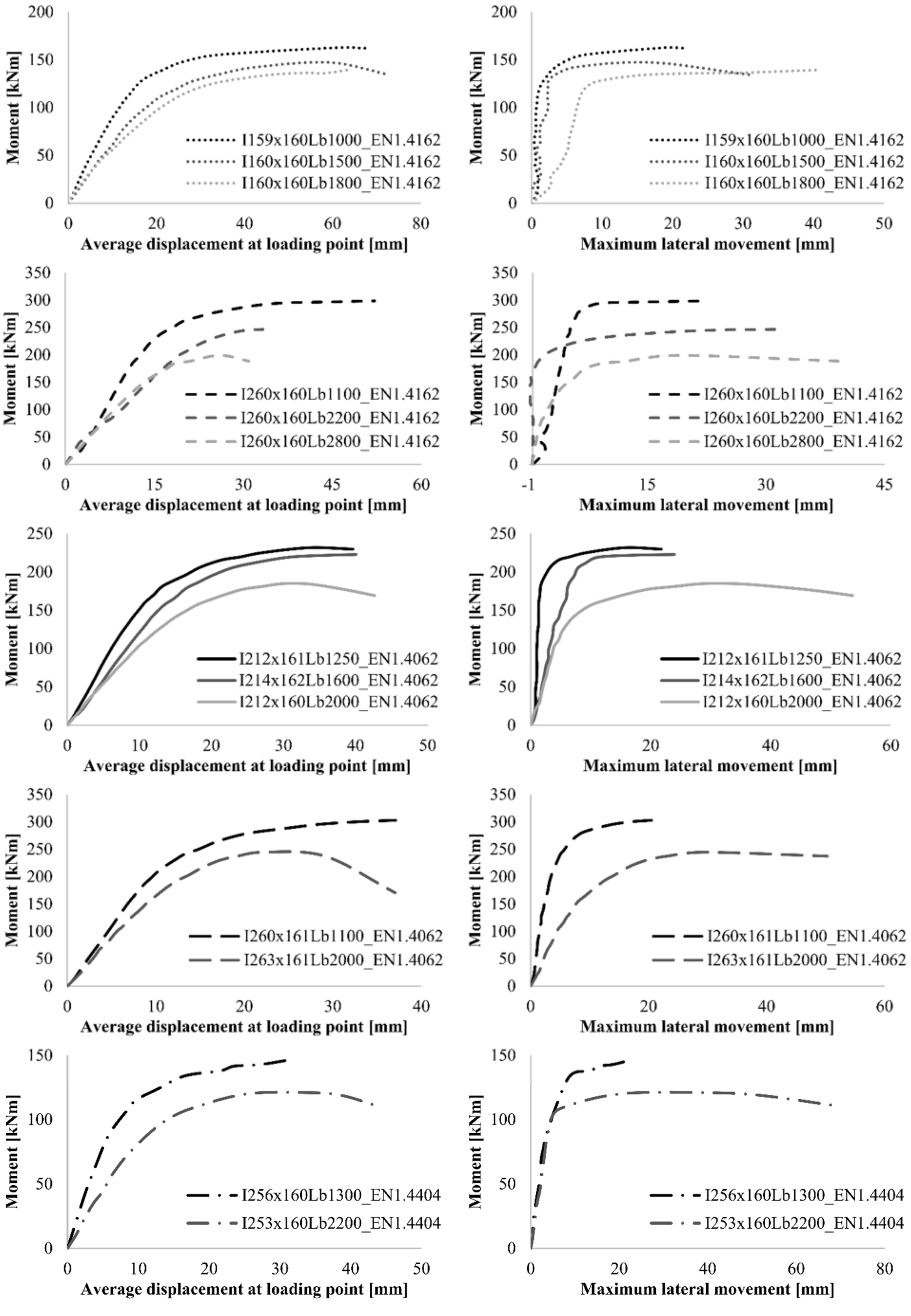

Figure 14: Overview of the displacement of the loading points compared to the applied moment for all tests.

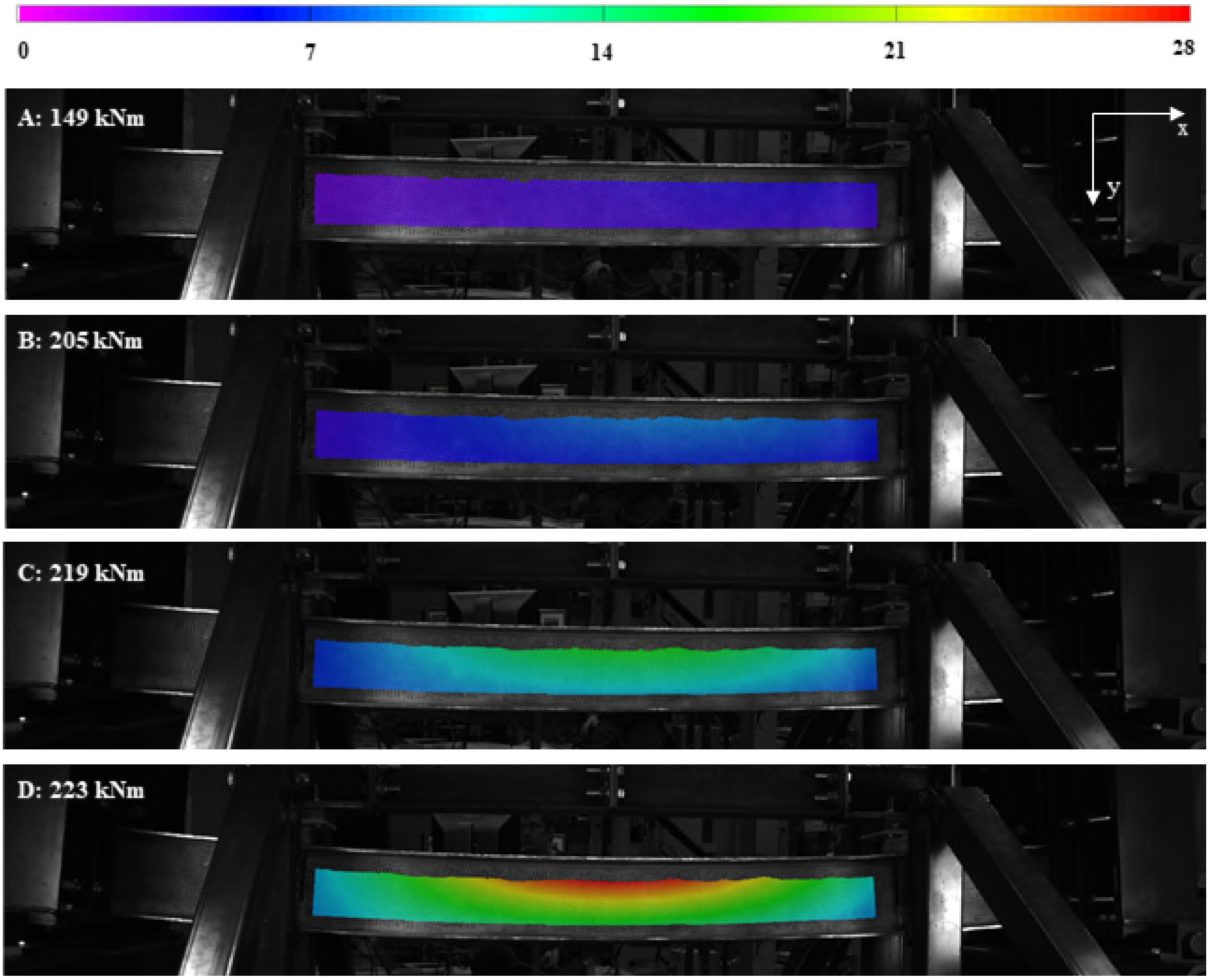

Figure 15: Out-of-plane displacement during test I214x162Lb1600_EN1.4062

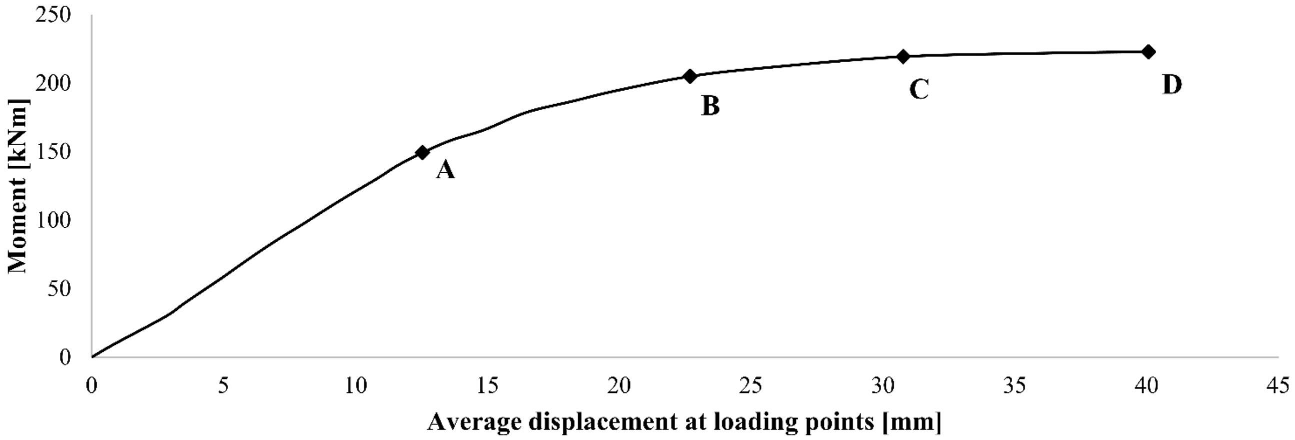

Figure 16: Vertical displacement of the loading points compared to the applied moment for I214x162Lb1600_EN1.4062

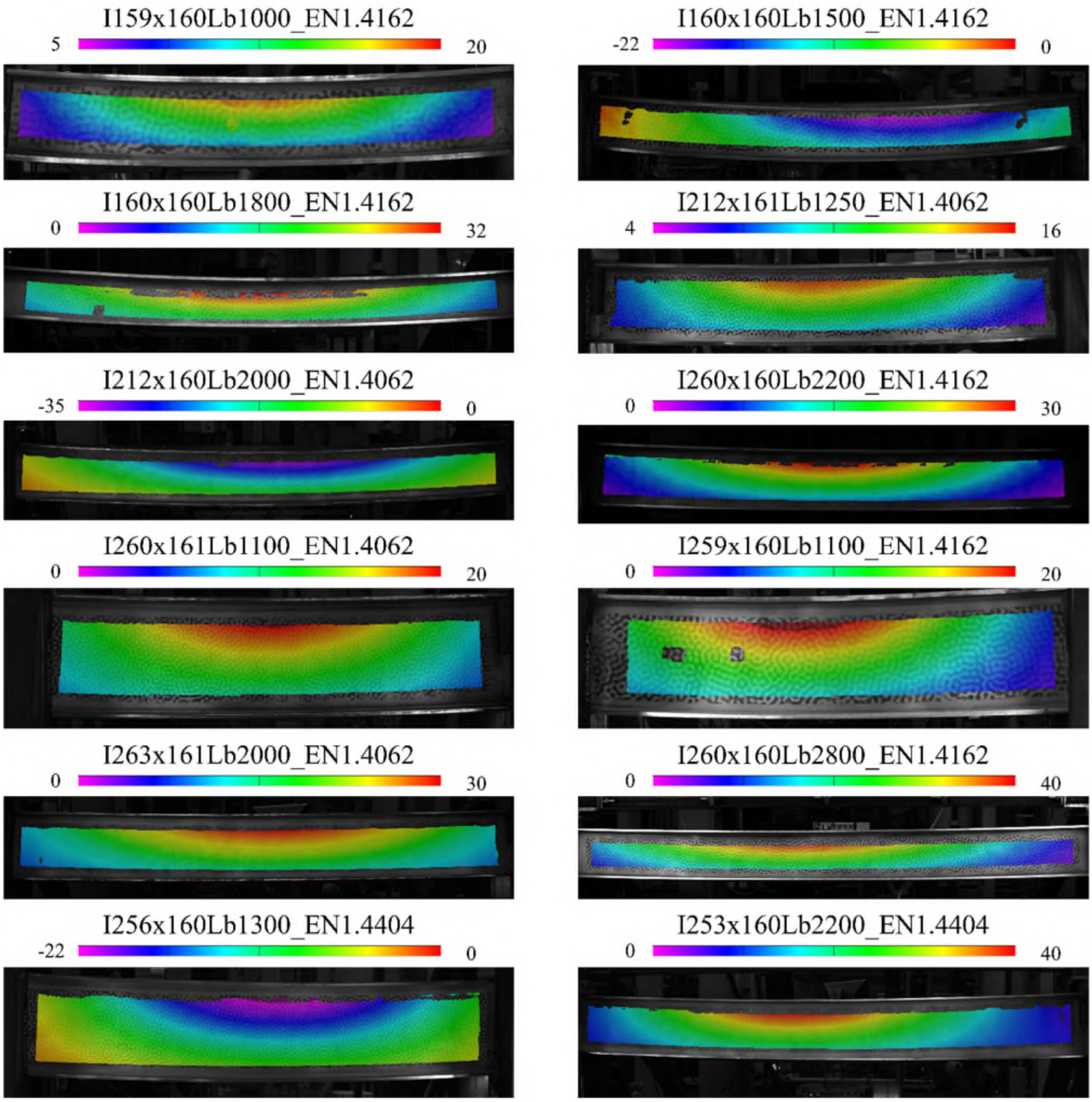

Figure 17: Out-of-plane displacement measured with DIC for all beams at ultimate load.

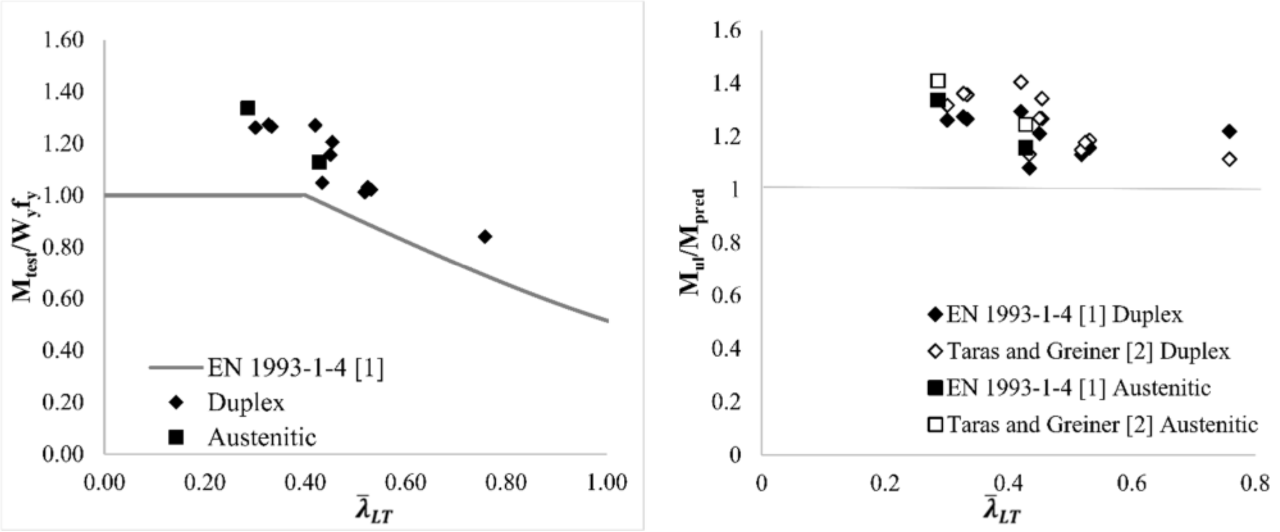

Figure 18: Comparison of the ultimate moment to the predicted moment according to EN 1993-1-4 and Taras and Greiner.